Efficient Metamorphosis Computation for Classifying Embryonic Cardiac Action Potentials

Giann Gorospe[1], Renjun Zhu[1], Jia-Qiang He[2], Leslie Tung[1], Laurent Younes[1], and René Vidal[1]

[1] Johns Hopkins University, Baltimore, USA
[2] Virginia Tech University, Blacksburg, USA

Abstract. As purification methods for obtaining cardiomyocytes from stem cells continue to improve, the need for automated methods for high-throughput classification of these cells is becoming extremely important. Since the shape of the action potential of an adult cell is discriminative of its phenotype, a promising classification approach is to use the metamorphosis distance between the action potentials of embryonic and adult cells. However, current gradient descent methods for computing the metamorphosis distance are extremely slow, hence unsuitable for large scale classification. In this paper, we show that the metamorphosis path can be computed in closed form given the velocity field, which leads to an efficient alternating minimization approach for computing the metamorphosis distance. We test this algorithm on heart cell datasets varying from 100 to 7,000 cells.

Keywords: Cardiac electrophysiology, shape analysis, machine learning

1 Introduction

Ever since Kehat et al. [1] pioneered cardiomyocyte differentiation back in 2001, there has been a lot of hope in the potential of stem cell based cardiology. This dream was bolstered further by the work of [2], which showcased the medical potential for human embryonic stem cell derived cardiomyocytes in infarcted rat hearts. The goal of utilizing stem-cell derived cardiomyocytes for cardiac regeneration, as well as disease models [3] could prove instrumental to the future of cardiology. However, as expressed in multiple texts [4, 5], there is still a need for methods to identify cardiomyocyte phenotype (nodal, atrial, or ventricular) in order to prevent potential arrhythmias, improve sustained cardiac regeneration, or to provide consistent models for therapeutic study.

In 2003, [6] showed that stem cell derived cardiomyocytes could be divided into several phenotypes based on their electrophysiological signature, called an action potential (AP). They labelled the three phenotypes embryonic nodal-like, embryonic atrial-like, and embryonic ventricular-like. Examples of the embryonic atrial-like and embryonic ventricular-like APs are provided in Figure 1. They determined this classification manually, and verified it by obtaining measurements

of features of the action potentials, such as action potential amplitude and duration, and showing statistically significant differences between the phenotypes. Other works [7, 8] have used similar processes for classification. The problem with classification methods of this type is that they are subjective, which makes them difficult to transfer across datasets, where acquisition protocols may be different.

We believe that automated, objective methods for embryonic heart cell classification are integral to the study of embryonic cardiomyocytes. However, the development of classification methods faces several fundamental challenges. First, the selection of shape features for classification is only well understood in the case of adult cells, and continues to be an art. Second, the phenotypes of immature cells need not coincide with the phenotype of adult cells, and even if they do, the shape of the action potential may change throughout the maturation process. Understanding the morphological changes of the AP during maturation may prove insightful to the underlying cellular processes.

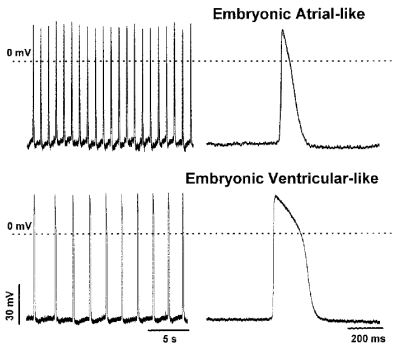

Fig. 1. Sample embryonic action potentials as described by [6]

As these embryonic cardiomyocytes will eventually become one of the mature phenotypes of interest to clinicians, determining the fate and maturation process of an embryonic cardiomyocyte from the shape of the AP will help reduce the potential risks in future studies. We would like a model that not only provides a way to determine the mature fate of the embryonic cardiomyocyte, but also provides insight into the modification of the AP as it matures from infancy to adulthood. While there is limited evidence of the maturation process, the general hypothesis is that the action potential evolves smoothly from infancy to maturity. Thus, smooth deformation models, like the metamorphosis distance, introduced in [9–11] and applied in [12] to cardiomyocyte classification, is a promising approach to address these challenges. However, while [12] showed very promising results on using the metamorphosis distance for action potential classification, the method used for computing the distance is computationally inefficient. As cardiomyocyte differentiation methods mature, and larger populations of cells become available, there is a need for faster approaches for computing the metamorphosis distance.

The main contribution of this paper is to propose an alternative method for computing the discrete metamorphosis model. Given two action potentials, the metamorphosis is obtained by finding the optimal interpolant and deformation paths that interpolate the two action potentials, warping one into the other. Rather than solving the optimization problem by gradient descent, we show that the optimal interpolant path for a given velocity field can be computed in closed form. Our experiments show that this leads to a slightly more efficient

alternating minimization approach for computing the metamorphosis distance, which requires fewer iterations and perfoms better compared to gradient descent methods. We demonstrate the performance of the proposed algorithm on a small microelectrode recording dataset of about 100 action potentials and, for the first time, on a large optical mapping dataset of about 7,000 action potentials.

2 Review of Metamorphosis

The metamorphosis distance, proposed in [10] and [11], is an interpolation scheme used for defining a Riemannian distance between two shapes. In this section, we will review this scheme in the context of cardiac action potentials, which are one dimensional shapes. However, this scheme may be applicable to other shapes.

Let $I_0(\tau)$ and $I_1(\tau)$ be two action potentials, called, respectively, template and target. We assume that these signals are periodic, continuously differentiable and square integrable, i.e., $I_0, I_1 \in L^2(\mathcal{S}^1)$, where $\mathcal{S}^1$ is the unit circle. A metamorphosis is a family of action potentials $\{I(\cdot,t) \in L^2(\mathcal{S}^1)), t \in [0,1]\}$ that interpolates between the template $(I(\tau,0) = I_0(\tau))$ and the target $(I(\tau,1) = I_1(\tau))$. Each element of this family can be further decomposed in terms of a diffeomorphism $\phi(\cdot,t) \in \mathrm{Diff}(\mathcal{S}^1)$ acting on an evolving template $i(\tau,t)$ as

$$I(\tau,t) = \phi(\tau,t) \cdot i(\tau,t) = i(\phi^{-1}(\tau,t),t). \tag{1}$$

To define a distance between two action potentials using this model, we need to define an energy that depends on the infinitesimal change in the deformation $(\frac{\partial \phi}{\partial t})$ and the infinitesimal change in the template $(\frac{\partial i}{\partial t})$. Because ϕ is a diffeomorphism, we can define the infinitesimal change in the deformation $\frac{\partial \phi}{\partial t}$ by a smooth flow field v $(\frac{\partial \phi}{\partial t} = v(\phi(\tau,t),t))$ and penalize its smoothness with a Sobolev norm (a norm on a function and its derivatives). For example, let $L(\cdot)$ is a linear differential operator acting on v (for example, $Lv = v - \alpha \frac{\partial^2}{\partial \tau^2} v$). We can use a Sobolev norm that can be expressed in terms of the Euclidean norm as:

$$\left\| \frac{\partial \phi}{\partial t} \right\|_V^2 = \|v\|_V^2 = \langle v, Lv \rangle. \tag{2}$$

On the other hand, we can compute the infinitesimal change in the template by taking the derivative of $I(\tau,t)$ with respect to t, which gives (see [11] for the details):

$$\frac{\partial i}{\partial t} = \frac{\partial I}{\partial t} + \frac{\partial I}{\partial \tau} v, \tag{3}$$

and then penalize this change using its Euclidean distance. Combining the two penalties with a balancing parameter σ allows us to define an energy on the family, which can be minimized over all families to define a distance between template and target as:

$$d^2_{\mathcal{M}}(I_0, I_1) = \inf_{\substack{v,I \\ I(\tau,0)=I_0(\tau) \\ I(\tau,1)=I_1(\tau)}} \int_0^1 \left(\frac{1}{2} \|v(\tau,t)\|_V^2 + \frac{1}{2\sigma^2} \left\| \frac{\partial I}{\partial t}(\tau,t) + \frac{\partial I}{\partial \tau}(\tau,t)\, v(\tau,t) \right\|_{L^2}^2 \right) dt. \tag{4}$$

One approach to minimizing this distance is to discretize the energy, and then develop methods to minimize the resulting discretized energy. For example, [12] and [13], take advantage of the following approximation to discretize τ:

$$\int_0^1 \left\| \frac{\partial I}{\partial t}(\tau,t) + \frac{\partial I}{\partial \tau}(\tau,t)v(\tau,t) \right\|_{L_2}^2 dt \approx \sum_{k=0}^{S-1} \left\| \frac{I(t+\delta t v(\tau,t_k),t_{k+1}) - I(\tau,t_k)}{\delta t} \right\|_{L_2}^2. \tag{5}$$

After combining this with a discretization for τ, the energy becomes:

$$E(v(\tau_i,t_k),I(\tau_i,t_k)) = \sum_{k=0}^{S-1} \frac{1}{2}\|v(\tau_i,t_k)\|_V^2 + \frac{1}{2\sigma^2}\|I(\tau_i+v(\tau_i,t_k),t_{k+1})) - I(\tau_i,t_k)\|_{l_2}^2. \tag{6}$$

Both [12] and [13] minimize this discrete energy via alternating gradient descent. In particular, following [12], let L_d be the discretized version of the linear operator in (2), and let $K = L_d^{-1}$ be the corresponding smoothing kernel for the derivative operator L_d. Now, using $w = L_d^{1/2}v$, the gradient of E with respect to this new variable w at each interpolation step can be calculated via the chain rule as:

$$\frac{\partial E}{\partial w(\tau_i,t_k)} = w(\tau_i,t_k) + \frac{1}{\sigma^2}K^{1/2}(I(\bar{\tau}_i,t_{k+1}) - I(\tau_i,t_k))\frac{\partial I(\bar{\tau}_i,t_{k+1})}{\partial \tau_i}, \tag{7}$$

where $\bar{\tau}_i = \tau_i + K^{1/2}w(\tau_i,t_k)$.

Now, given w, and as a result, v, the gradient update of the metamorphosis interpolants, $I(\tau,t_k)$ can be determined by making an approximation. Since we are discretizing in the "spatial" domain τ, we sample each $I(\tau,t_k)$ and specific points τ_i. Thus, when we look at $I(\tau+v(\tau,t_k),t_{k+1})$, it is likely that $\tau_i+v(\tau_i,t_k)$ does not coincide with the original samples τ_i. Therefore we have to approximate the value of $I(\tau_i+v(\tau_i,t_k),t_{k+1})$ in terms of the samples original discretization $I(\tau_i,t_{k+1})$ so that they can be compared to the samples of $I(\tau_i,t_k)$. The action of approximating the sampling of $I(\tau+v(\tau,t_k),t_{k+1})$ using the samples of $I(\tau,t_{k+1})$ is denoted by the operator N_{v_k} and is realized by the linear interpolation matrix:

$$N_{v_k}I(\tau,t_{k+1}) \approx I(\tau+v(\tau,t_k),t_{k+1}). \tag{8}$$

This leads to:

$$E(I(\tau,t)) \approx \sum_{k=0}^{S-1} \frac{1}{2\sigma^2}\|N_{v_k}I(\tau,t_{k+1}) - I(\tau,t_k)\|_{L^2}^2. \tag{9}$$

The gradient with respect to $I(\tau,t_k), k = 1,\ldots,S-1$, is given by:

$$\frac{\partial E}{\partial I(\tau,t_k)} = \frac{1}{\sigma^2}(N_{v_{k-1}}^T(N_{v_{k-1}}I(\tau,t_k) - I(\tau,t_{k-1})) - (N_{v_k}I(\tau,t_{k+1}) - I(\tau,t_k))). \tag{10}$$

While alternating between updates of v and I does find a local minimum to the optimization problem, the gradient descent steps are handcuffed by the choice of the step size. This can be addressed by either finding an appropriate adaptive step size, or by a large number of iterations at a fixed, but stably small step size. However, both schemes require additional computational effort.

3 A Closed Form Update for Continuous Metamorphosis

If the goal is a model of maturation and classification of large populations of cardiomyocytes, it will be difficult to scale gradient descent methods for solving tens of thousands of optimization problems. In this paper, we propose an alternative approach in which the solution for some variables can be computed in closed form given the other variables. To motivate the proposed approach, in this section we present a formulation derived in [14] for solving the alternating minimization updates of the continuous energy in (4). In the next section, we will show how this approach can be extended to the discrete energy.

We begin by applying the chain rule to compute the variation of the energy in (4) with respect to v. This leads to an update for $v(\tau,t)$ with fixed $I(\tau,t)$ that is based on solving the following non-homogeneous differential equation:

$$\Big(2L + \frac{1}{\sigma^2}\Big(\frac{\partial I}{\partial \tau}(\tau,t)\Big)^2\Big)v(\tau,t) = \frac{1}{\sigma^2}\Big(-\frac{\partial I}{\partial t}(\tau,t)\frac{\partial I}{\partial \tau}(\tau,t)\Big), \tag{11}$$

where $Lv = v - \alpha\frac{\partial^2}{\partial \tau^2}v$. Now, alternatively, minimizing this distance with respect to $I(\tau,t)$, with $v(\tau,t)$ fixed, leads to minimizing the following energy:

$$E(I(\tau,t)) = \int_0^1 \frac{1}{2\sigma^2}\Big\|\frac{\partial I}{\partial t}(\tau,t) + \frac{\partial I}{\partial \tau}(\tau,t)\ v(\tau,t)\Big\|_{L^2}^2 dt. \tag{12}$$

Taking the variation with respect to $I(\tau,t)$ leads to a complicated differential equation to be solved. However, if we instead let $J(\tau,t) = I(\phi(\tau,t),t)$ and $u = \phi^{-1}(\tau,t)$, then it is not difficult to show that differentiating $J(\tau,t)$ with respect to t leads to the following result:

$$\frac{\partial J(\phi^{-1}(\tau,t),t)}{\partial t} = \frac{\partial I(\tau,t)}{\partial t} + \frac{\partial I(\tau,t)}{\partial \tau}v(\tau,t). \tag{13}$$

After making the change of variables $u = \phi^{-1}(\tau,t)$ and substituting the above relationship, the energy becomes:

$$E(J(u,t)) = \int_0^1 \|\frac{\partial J(u,t)}{\partial t}\|_{L^2}^2 \frac{\partial \phi(u,t)}{\partial u}dt. \tag{14}$$

The Gateaux variation of E with respect to J, and setting it to 0 leads to:

$$J(u,t) = J(u,0)\frac{\int_t^1 \frac{1}{\frac{\partial \phi(u,t')}{\partial u}}dt'}{\int_0^1 \frac{1}{\frac{\partial \phi(u,t')}{\partial u}}dt'} + J(u,1)\frac{\int_0^t \frac{1}{\frac{\partial \phi(u,t')}{\partial u}}dt'}{\int_0^1 \frac{1}{\frac{\partial \phi(u,t')}{\partial u}}dt'}. \tag{15}$$

After computing $J(u,t)$, one may obtain $I(\tau,t)$ by back-substitution. Thus, not only it is possible to compute the optimal $I(\tau,t)$ given $v(\tau,t)$ in closed form, the optimal solution is essentially a weighted combination of the source and the target. In practice, however, the update for v given I and vice versa cannot be implemented without first discretizing the equations, as discussed next.

4 A Closed Form Update for Discrete Metamorphosis

One approach to implementing the updates for v and I described in the previous section is to simply discretize the updates. However, a naive discretization of the continuous updates need not coincide with the updates for a discretization of the original objective, such as that in (6). In this section, we derive closed form updates for the minimization of the discrete energy in (6).

4.1 Formulation

Let $N_k = N_{v_k}$ and $I_k = I(\tau, t_k)$. If $Z_k = N_k I_{k+1} - I_k$, then at the optimum, (10) simplifies to:

$$Z_k = N_{k-1}^T Z_{k-1} \tag{16}$$

If we let $R_{i,j} = N_i N_{i+1} \dots N_{j-1}$, it follows that $Z_k = R_{0,k}^T Z_0$. Using this, and the original definition of Z_k, we can write an equation for I_k:

$$I_k = N_k I_{k+1} - Z_k = N_k I_{k+1} - R_{0,k}^T Z_0. \tag{17}$$

Iterating backwards from $k = S-1$, we can write these equations using I_S as:

$$I_k = R_{k,S} I_S - (\sum_{i=k}^{S-1} R_{k,i} R_{0,i}^T) Z_0 = R_{k,S} I_S - A_{k,S} Z_0, \tag{18}$$

where $A_{l,m} = \sum_{i=l}^{m-1} R_{l,i} R_{0,i}^T$. To determine Z_0, we look at I_0:

$$I_0 = R_{0,S} I_S - A_{0,S} Z_0 \implies Z_0 = A_{0,S}^{-1}(R_{0,S} I_S - I_0). \tag{19}$$

So, after replacing Z_0, we find an update for I_k that depends only on I_0 and I_S:

$$I_k = A_{k,S} A_{0,S}^{-1} I_0 + (R_{k,S} - A_{k,S} A_{0,S}^{-1} R_{0,S}) I_S. \tag{20}$$

4.2 Computation

From (20), we get a closed form update for the interpolants I_k in terms of the template I_0 and target I_S. The next major question to solve is how to efficiently compute this update. Looking at the equation, we need $R_{k,S}$ and $A_{k,S}$ for all k. But given the current definition, $A_{k,S}$ requires knowledge of all $R_{i,j}$. This is

a large computational storage overhead, but it can be avoided by noticing that $A_{k,S}$ can also be determined using backwards iteration:

$$A_{k,S} = \sum_{i=k}^{S-1} R_{k,i} R_{0,i}^T = R_{0,k}^T + N_k A_{k+1,S}. \tag{21}$$

Thus we have the following system of forward and backwards updates:

$$I_k = B_{k,S} I_0 + (R_{k,S} - B_{k,S} R_{0,S}) I_S \tag{22}$$

$$R_{k,S} = N_k R_{k+1,S} \tag{23}$$

$$C_{0,k}^T = N_k^T C_{0,k-1}^T \tag{24}$$

$$B_{k,S} = C_{0,k}^T + N_k B_{k+1,S}, \tag{25}$$

where $B_{k,S} = A_{k,S} A_{0,S}^{-1}, C_{0,k}^T = R_{0,k}^T A_{0,S}^{-1}$. The initial conditions for the updates are: $R_{S,S} = Id$, $C_{0,0}^T = A_{0,S}^{-1}$, and $B_{S,S} = 0$. Here, $A_{0,S}^{-1}$ can be computed by using the original definition and the storage of $R_{0,k}$ which then can be used to generate $C_{0,k}$. Since the biggest computational task in this update is computing $A_{0,S}^{-1}$, the update of $A_{0,S}^{-1}$ can be done once every n iterations if a faster approximation is required. Our update for velocity follows that of [12]. The overall algorithm is presented in Algorithm 1. We acknowledge that this step is still gradient descent, and may be a limiting step in performing the overall algorithm. Finding a closed form solution for this optimization problem is difficult given the nonlinearity in v of the template evolution summand of the energy. Alternative approaches to performing this update more efficiently are a future research direction.

4.3 Convergence to continuous formulation

We have derived a closed form update for the metamorphosis interpolants, and provided a way to efficiently compute this optimum using forward-backward schemes. We comment now on how this proposed update relates to the continuous formulation. We omit many of the details here, but they can be found in the Supplementary Material. The convergence result can be summarized by the following theorem:

Theorem 1. *Let $I_k, k = 0, \ldots, S$, be the metamorphosis interpolants derived from* (20)*, and let $I(\tau, t)$ be the family of interpolants derived from $J(u, t)$ given by* (13)*. Then, as $S \to \infty$, $I_k \to I(\tau, t)$.*

Sketch of the Proof: Given that J represents the interpolants in the template domain, it follows that the discrete version J_k of I_k is $J_k = R_{0,k} I_k$. Proceeding from $I_k = A_{k,S} A_{0,S}^{-1} I_0 + (R_{k,S} - A_{k,S} A_{0,S}^{-1} R_{0,S}) I_S$, it is not difficult to show that $J_k = (Id - A_{0,k} A_{0,S}^{-1}) J_0 + A_{0,k} A_{0,S}^{-1} J_S$. From here, after some analysis one can show $R_{0,k}(J(\cdot, t)) \to J(\phi(\cdot, \frac{k}{S}), t)$, which leads to the result.

Algorithm 1 Discrete Metamorphosis via Direct Image Computation

Given a Template Signal $I_0(\tau)$, a Target Signal $I_1(\tau)$, a balance parameter σ, the number of evolution time steps S, and a Sobolev Operator L_d, update frequency n.

1. Initialization.
   (a) Set $m = -1$, $d_{-1} = \infty$. Calculate $K = L_d^{-1}$.
   (b) Set $w(\tau_i, t_k) \equiv 0$, $v(\tau_i, t_k) = K^{1/2} w(\tau_i, t_k) \equiv 0$, for all t_k and τ_i.
   (c) For $k = 0, \ldots, S$: Set $I(\tau_i, t_k) = \frac{S-k}{S} I_0(\tau_i) + \frac{k}{S} I_1(\tau_i)$
   (d) Calculate $d_0^2 = \sum_{k=0}^{S-1} \frac{1}{2} \|w(\tau_i, t_k)\|_{l_2}^2 + \frac{1}{2\sigma^2} \|N_{v_k} I(\tau_i, t_{k+1})) - I(\tau_i, t_k)\|_{l_2}^2$
2. Until $d_{m-1} - d_m$ converges
   (a) Set $d_m \to d_{m-1}, m + 1 \to m$.
   (b) For $k = 0, \ldots, S-1$, Update $w(\tau_i, t_k)$ using (7).
   Calculate $v(\tau_i, t_k) = real(K^{1/2} w(\tau_i, t_k))$, Update N_{v_k}.
   Compute $R_{0,k}$ and $R_{k,S}$ for $k = 0, \ldots, S$.
   (c) if $\mathrm{mod}(m, n) = 0$,
   Calculate $A_{0,S} = \sum_{i=0}^{S-1} R_{0,i} R_{0,i}^T$, Calculate $A_{0,S}^{-1}$.
   (d) Initialize $C_{0,0}^T = A_{0,S}^{-1}$, $B_{S,S} = 0$. Calculate:
   $C_{0,k}^T = N_k^T C_{0,k-1}^T$
   $B_{k,S} = C_{0,k}^T + N_k B_{k+1,S}$
   $I_k = B_{k,S} I_0 + (R_{k,S} - B_{k,S} R_{0,S}) I_S$
   (e) Calculate $d_m^2 = \sum_{k=0}^{S-1} \frac{1}{2} \|w(\tau_i, t_k)\|_{l_2}^2 + \frac{1}{2\sigma^2} \|N_{v_k} I(\tau_i, t_{k+1})) - I(\tau_i, t_k)\|_{l_2}^2$

5 Experiments

5.1 Patch Clamp Data

In this section, we evaluate the efficiency of our algorithm by comparing it to the gradient descent based method proposed in [12] on the dataset generated by [6]. The dataset contains 16 embryonic atrial-like and 36 embryonic ventricular-like cardiomyocytes, manually labeled according to [6] based on AP features. The data was pre-processed using the protocol described in [12]. Namely, we fixed the cycle length to 1 second using the algorithm presented by [15]. For classification purposes, we generated 10 mature atrial and 10 mature ventricular protoype action potentials using the atrial model of [16] and the ventricular model of [17], respectively. All signals were then normalized so that the resting membrane potential has voltage 0, and the amplitude has voltage 1.

We computed the metamorphosis distance from each of the embryonic cardiomyocytes to each one of the mature prototypes. We used the linear operator $L_d(\cdot) = id(\cdot) - \alpha\Delta(\cdot)$, with $\alpha = 8$, and set the parameterσ to 0.3 and the number of interpolants between template and target to 3 ($S = 4$). We iterated our algorithm and that of [12] until they reached convergence or 300 iterations.

Figure 2 compares the method of [12] and two variants of our method (with $A_{0,S}^{-1}$ updated each iteration or every 10 iterations) in terms of the final interpolations and the distances they produce. We see that there is very little difference between the three interpolations, and that the three distances are approximately equal. The main difference is that our method with $A_{0,S}^{-1}$ updated every 10 iterations requires about half the number of iterations than the other methods.

(a) Gradient Descent Metamorphosis [12]: $d^2_{\mathcal{M}} = 206.8240$, Iterations: 74

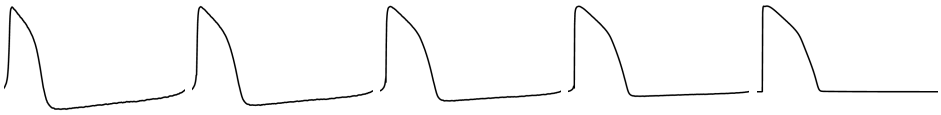

(b) Proposed method, $A^{-1}_{0,S}$ updated every iteration: $d^2_{\mathcal{M}} = 208.2602$, Iterations: 72

(c) Proposed method, $A^{-1}_{0,S}$ updated every 10 iterations: $d^2_{\mathcal{M}} = 207.6308$, Iterations: 38

Fig. 2. Comparison of the metamorphosis method in [12] and two variants of the proposed method in terms of the interpolants and the distances they compute.

Table 1 compares the the Euclidean distance, the metamorphosis distance computed with the method in [12], and the metamorphosis distance computed using the two variants of our method in terms of their classification performance and computation time on the entire dataset. For this purpose, we use the 20 mature prototypes as our training set, and the entire dataset as the test set. Classification is done with the 1 nearest neighbor (NN) and 3 NN classifiers, meaning we classify an AP based on the class of the closest 1 or 3 mature prototypes. While the Euclidean distance is the fastest to compute, the classification performance is better using the metamorphosis distance. Moreover, we see that our method provides improved classification rate relative to the current state-of-the-art method at reduced computation time. In fact, when $n = 10$, the computation time is almost completely in the gradient descent update for v, suggesting that the computational limit in the interpolant update has been reached. While improving the speed of the velocity updates is one of our future research goals, the findings on this dataset suggest that our algorithm provides an improvement over the current standard.

5.2 Optical Data

We also tested our algorithm on a much larger dataset consisting of 9 cell clusters with APs recorded using the optical mapping technique of [18]. The number of APs in each cell cluster ranges from 400 to 1000, and the total number of APs in the dataset equals 6940. Mature prototypes were generated using the same computational models as in the previous experiment. The signals were paced at

Table 1. Comparison of the metamorphosis method in [12] and two variants of the proposed method in terms of classification performance and computation time on a patch clamp dataset.

	Euclidean Distance	Gorospe et al. [12]	Our Method (n = 1)	Our Method (n = 10)
1 NN Atrial Scoring	**16**/16	13/16	14/16	14/16
1 NN Ventricular Scoring	29/36	**36**/36	**36**/36	**36**/36
3 NN Atrial Scoring	**16**/16	13/16	14/16	14/16
3 NN Ventricular Scoring	29/36	**36**/36	**36**/36	**36**/36
Computation Time (in seconds)	$< \mathbf{1}$	17.0181	15.8265	12.0815

a rate of 1.5 Hz (cycle length of $\frac{2}{3}$ seconds), and also normalized to have resting potential voltage 0, and maximum voltage amplitude of 1.

We computed the metamorphosis distance using our new formulation with $n = 1$ from each AP in the dataset to each one of the mature prototypes using the same parameters as in the patch clamp experiment. The algorithms were run in 2 8-core computer nodes with 8 hyperthreaded 2.3 GHz CPUs per node. The total time to complete the analysis on the entire dataset was 13 hours, with individual cell clusters taking between 50 and 80 minutes.

Figure 3 compares the classification results obtained by a 1-NN classifier with the Euclidean distance versus the metamorphosis distance for each one of the 9 cell clusters. We omit the 3 NN results as the results are identical. The blue color indicates areas where the APs were classified as atrial, and red indicates areas that were classified as ventricular. While some of the cell clusters present with only 1 phenotype, the majority of the cell clusters present with both phenotypes in varying concentrations, affirming recent work [19].

Figure 3(c) compares the action potentials of the cell clusters obtained by a 1-NN classifier with the Euclidean and Metamorphosis distances for a pair of heterogeneous clusters. For the metamorphosis classification, the two classes show distinct shapes, and they are similar to those described by [6] for embryonic atrial-like and embryonic ventricular-like. In comparison, the Euclidean classification fails to capture the distinction between the phenotypes. This affirms that the metamorphosis distance is a suitable automated counterpart to manual classification by biologists. More importantly, it suggests that the metamorphosis model could be used to reliably assess the phenotype statistics of populations of APs. As a consequence, the metamorphosis model may prove insightful to a growing collection of methods that have been derived to isolate a particular phenotype of embryonic cardiomyocytes [20, 21].

6 Conclusion

We have presented an algorithm for computing the metamorphosis that performs comparably with the current state of the art, but at approximately two-thirds the run time. We presented a closed form update for the interpolants that can be computed via a series of forward and backwards updates, as well as demon-

(a) Euclidean 1-NN

(b) Metamorphosis 1-NN

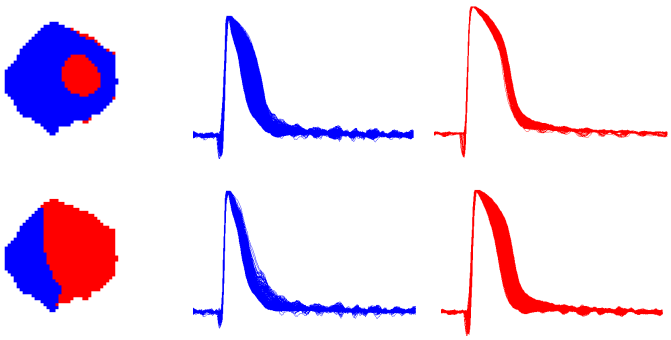

Classified Cell Cluster Atrial Signals Ventricular Signals

(c) Cell cluster classifications and their corresponding action potentials.

Fig. 3. Comparison of the Euclidean distance and the metamorphosis distance for 1-NN classification of the optical dataset.

strated its convergence to the continuous evolution metamorphosis updates. We demonstrated its effectiveness on a studied microelectrode recording dataset, as well as a much larger scale optical mapping dataset. We believe that the new method could lead to advances in stem cell cardiology, as well as lead to potential new frontiers in computational shape analysis.

References

1. Kehat, I., Kenyagin-Karsenti, D., Snir, M., Segev, H., Amit, M., Gepstein, A., Livne, E., Binah, O., Itskovitz-Eldor, J., Gepstein, L.: Human embryonic stem cells can differentiate into myocytes with structural and functional properties of cardiomyocytes. Journal of Clinical Investigation **108**(3) (2001) 407–414
2. Laflamme, M.A., Chen, K.Y., Naumova, A.V., Muskheli, V., Fugate, J.A., Dupras, S.K., Reinecke, H., Xu, C., Hassanipour, M., Police, S., O'Sullivan, C., Collins, L., Chen, Y., Minami, E., Gill, E.A., Ueno, S., Yuan, C., Gold, J., Murry, C.E.: Cardiomyocytes derived from human embryonic stem cells in pro-survival factors enhance function of infarcted rat hearts. Nature Biotech. **25**(9) (2007) 1015–24
3. Hoekstra, M., Mummery, C.L., Wilde, A.A., Bezzina, C.R., Verkerk, A.O.: Induced pluripotent stem cell derived cardiomyocytes as models for cardiac arrhythmias. Frontiers in Physiology **3**(346) (2012)

4. Maher, Kevin O. andi Xu, C.: Marching Towards Regenerative Cardiac Therapy with Human Pluripotent Stem Cells. Discovery Medicine **15** (2013) 349–356
5. Xu, X.Q., Sun, W.: Perspective from the heart: The potential of human pluripotent stem cell-derived cardiomyocytes. Journal of Cellular Biochemistry **114**(1) (2013) 39–46
6. He, J.Q., Ma, Y., Lee, Y., Thomson, J.A., Kamp, T.J.: Human embryonic stem cells develop into multiple types of cardiac myocytes: action potential characterization. Circulation Research **93**(1) (2003) 32–9
7. Moore, J.C., Fu, J., Chan, Y.C., Lin, D., Tran, H., Tse, H.F., Li, R.A.: Distinct cardiogenic preferences of two human embryonic stem cell (hESC) lines are imprinted in their proteomes in the pluripotent state. Biochemical and biophysical research communications **372**(4) (2008) 553–8
8. Zhang, J., Wilson, G.F., Soerens, A.G., Koonce, C.H., Yu, J., Palecek, S.P., Thomson, J.A., Kamp, T.J.: Functional cardiomyocytes derived from human induced pluripotent stem cells. Circulation Research **104**(4) (February 2009) e30–41
9. Miller, M., Younes, L.: Group actions, homeomorphisms, and matching: A general framework. International Journal of Computer Vision **41**(1-2) (2001) 61–84
10. Trouvé, A., Younes, L.: Metamorphoses Through Lie Group Action. Foundations of Computational Mathematics **5**(2) (2005) 173–198
11. Younes, L.: Shapes and Diffeomorphisms. Volume 171 of Applied Mathematical Sciences. Springer (2010)
12. Gorospe, G., Younes, L., Tung, L., Vidal, R.: A metamorphosis distance for embryonic cardiac action potential interpolation and classification. In: Medical Image Computing and Computer Assisted Intervention. (2013) 469–476
13. Garcin, L., Younes, L.: Geodesic image matching: A wavelet based energy minimization scheme. Energy Minimization Methods in Computer Vision and Pattern Recognition (2005) 349–364
14. Trouvé, A., Younes, L.: Local geometry of deformable templates. SIAM Journal on Mathematical Analysis **37**(1) (2005) 17–59
15. Iravanian, S., Tung, L.: A novel algorithm for cardiac biosignal filtering based on filtered residue method. IEEE Transactions on Biomedical Engineering **49**(11) (2002) 1310–7
16. Nygren, A., Fiset, C., Firek, L., Clark, J., Lindblad, D., Clark, R., Giles, W.: Mathematical model of an adult human atrial cell: The role of K+ currents in repolarization. Circulation Research **82**(1) (1998) 63–81
17. O'Hara, T., Virág, L., Varró, A., Rudy, Y.: Simulation of the undiseased human cardiac ventricular action potential: model formulation and experimental validation. PLoS computational biology **7**(5) (2011)
18. Weinberg, S., Lipke, E.A., Tung, L.: In Vitro Electrophysiological Mapping of Stem Cells. Methods in Molecular Biology **660** (2010) 215–237
19. Gorospe, G., Zhu, R., Millrod, M., Zambidis, E., Tung, L., Vidal, R.: Automated grouping of action potentials of human embryonic stem cell-derived cardiomyocytes. IEEE Transactions on Biomedical Engineering (2014)
20. Zhang, Q., Jiang, J., Han, P., Yuan, Q., Zhang, J., Zhang, X., Xu, Y., Cao, H., Meng, Q., Chen, L., Tian, T., Wang, X., Li, P., Hescheler, J., Ji, G., Ma, Y.: Direct differentiation of atrial and ventricular myocytes from human embryonic stem cells by alternating retinoid signals. Cell Research **21**(4) (2011) 579–87
21. Zhang, X., Guo, J.P., Chi, Y.L., Liu, Y.C., Zhang, C.S., Yang, X.Q., Lin, H.Y., Jiang, E.P., Xiong, S.H., Zhang, Z.Y., Liu, B.H.: Endothelin-induced differentiation of Nkx2.5 cardiac progenitor cells into pacemaking cells. Molecular and Cellular Biochemistry **366**(1-2) (2012) 309–18